JACS
JOURNAL OF THE AMERICAN CHEMICAL SOCIETY

ARTICLE

pubs.acs.org/JACS

One-Step Synthesis of Hierarchical Zeolite Beta via Network Formation of Uniform Nanocrystals

Karin Möller,*[,†] Bilge Yilmaz,[‡] Richard M. Jacubinas,[‡] Ulrich Müller,[‡] and Thomas Bein*[,†]

[†]Department of Chemistry and Center for NanoScience (CeNS), University of Munich (LMU), Butenandtstrasse 11 (E), D-81377 Munich, Germany

[‡]Chemicals Research & Engineering, BASF SE, D-67056 Ludwigshafen, Germany

ABSTRACT: A hierarchical mesoporous network of zeolite beta with very high micropore as well as mesopore volume was synthesized without the need of a porogen at near 100% yield in the form of easily retrievable micrometer-sized particles. This was achieved by a dense-gel synthesis utilizing steam-assisted conversion (SAC) to induce a burst of nucleation. During the first phase of the synthesis, individual, evenly sized zeolite beta nanoparticles are formed that subsequently condense into a porous network displaying uniform mesopores. The final product consists of hierarchical self-sustaining macroscopic zeolite aggregates assembled from 20 nm crystalline domains of zeolite beta. The small size of the zeolite crystals in the resulting materials gives rise to mesopores with dominant pore sizes of about 13 nm. Large surface areas between 630 and 750 m^2/g and total pore volumes up to 0.9 mL/g were obtained without sacrificing the microporosity (usually larger than 0.20 mL/g). Crystallization conditions were optimized for different Si/Al ratios between 10 and 33. A complete conversion into hierarchical zeolite beta was achieved in only a few hours at 170−180 °C if the amount of water present during the steam-assisted conversion was adequately adjusted. This dense gel steam conversion process proves to be a highly efficient strategy for fabricating hierarchical zeolite beta networks in a single step.

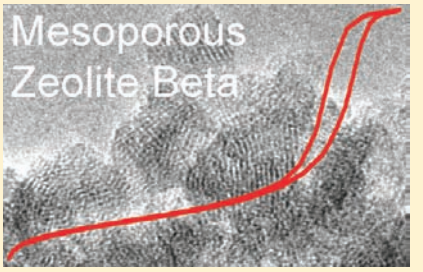

INTRODUCTION

Of the over 170 different zeolite structures known today, zeolite beta is one of the few examples that is of major importance in industrial applications.[1] Because of its three-dimensional architecture composed of intersecting 12-ring channels with large pores in combination with strong acidic sites, its applications comprise selective fine chemical conversions and catalytic crack reactions. Because many catalytic reactions are limited by constraints in mass-transfer, it is highly desirable to reduce the diffusion path of reactants and products in the zeolite phase. This quest has driven numerous activities in academics and industry in the past decade to design catalytically active microporous−mesoporous zeolite systems. Usually, cost- and time-intensive templating strategies or difficult postsynthetic modifications have been applied to achieve mesoporosity in these catalyst systems.[2−6] Generally, several strategies for the introduction of mesoporosity can be distinguished, including (i) soft templates in the form of surfactants or polymers, (ii) hard templates such as carbon- or resin-beads, or (iii) preformed biotemplates acting as scaffolds during synthesis, which are finally removed by subsequent calcination to leave their mesoporous imprint. Recently, even three-dimensionally ordered mesopores were beautifully arranged in a zeolitic matrix. Fan et al. carefully designed a multistep templating procedure allowing the alignment of silicalite nanoparticles in a porous carbon replica.[7] Alternatively, Choi et al. showed that with new bifunctional soft templates, containing micropore-directing diquaternary ammonium structures as well as mesopore directing organic partitions, it is possible to synthesize highly ordered multilamellar nanosheets of MFI.[8,9] An additional stabilization of these zeolite sheets through pillaring retained the mesoporous voids created by the surfactant tails even after calcination.[10] In another general approach, the mesoporosity is introduced into the zeolite phase after synthesis, using leaching methods in acidic or basic media.[11−14]

The synthesis of mesoporous zeolite beta materials has been approached by several of the methods mentioned above. Initially, the self-assembling mechanism of surfactant molecules to create mesoporous silica inspired the idea to convert the amorphous wall structure of these silicas into microporous zeolite beta. In an attempt to increase the stability and acidity of the mesoporous materials, the group of Pinnavaia et al. as well as the group of Xiao et al. used conditioned zeolite precursor solutions and reacted these with the amphiphilic templates.[15−17] They found truly mesoporous silicas containing zeolite-like substructures in the amorphous walls that were viewed as being responsible for the improved properties of these materials. Hierarchical systems were also obtained when mesoporous silica was used as a matrix for the dispersion of premade nanosized zeolites. Thus, Maschmeyer et al. added varying amounts of commercial nanobeta as additives to their TUD-1 mesoporous silica synthesis, increasing molecular access and stabilizing the nanoparticles against sintering.[18,19] Similarly, zeolite beta composite structures were made by Bagshaw et al.[20] They used zeolite seed solutions that

Received: September 27, 2010
Published: March 16, 2011

dx.doi.org/10.1021/ja108698s | *J. Am. Chem. Soc.* 2011, 133, 5284–5295

were briefly heated at temperatures common in zeolite beta synthesis (150 °C), subsequently quenched and adjusted in pH before being processed for a second time with a surfactant present. However, the materials made by amphiphilic surfactant templating suffer from the diluting presence of amorphous fractions, either as a segregated phase or as an embedding matrix for the microporous zeolite particles.

Meso- and microporosity has been obtained for zeolite beta when charged or neutral polymers were added as porogen during the zeolite synthesis. Xiao et al. used the cationic polymer polydiallyldimethylammonium chloride in a one-step procedure for zeolite beta[21] and achieved notable meso- (0.17 mL/g) and micropore volumes (0.16 mL/g).[22] In a subsequent study, introduction of a successively larger polymer fraction led to an increase in mesopore volume but simultaneously to a reduction of the zeolitic micropore volume.[23] Xiao and co-workers could further improve these results by using a two-step approach where a nanobeta solution was first prepared by heating the zeolite gel solution at 140 °C for 3 days.[24] In a second step, the polymer was added to this zeolite slurry and reacted for a second time under these conditions. This way, the authors achieved a high micropore volume (0.19 mL/g) as well as mesopore volume (0.84 mL/g) with a yield of 66%. The final material consisted of agglomerates of about 150 nm beta particles separated by smaller, about 20 nm crystals, giving rise to a total surface area of about 600 m^2/g. Zhu et al. applied a convenient one-step process using a polyvinyl butyral gel. Single crystals of zeolite beta of about 100−200 nm diameter were obtained with intracrystallite mesopores, showing a comparatively low porosity (e.g., 0.16 mL/g micropore and 0.36 mL/g mesopore volume, respectively, and a surface area of 447 m^2/g).[25]

More involved strategies using hard scaffolds have been applied in the zeolite beta synthesis.[26] Trimodal monolithic zeolite beta was prepared using a bimodal silica that was either stabilized via a carbonization route[27] or impregnated with the cationic polymer polydiallyldimethylammonium, and subsequently treated with a separately prepared nanozeolite beta suspension.[28] The resulting total pore volume including macropores ranged from 0.3 to 0.6 mL/g; however, relatively low micropore volumes (0.106−0.18 mL/g) and BET surface areas (380−560 m^2/g) were obtained. Furthermore, sacrificial resin beads have been used as macro-templates to prepare zeolite beta beads with 35 nm pores and high surface areas of about 640 m^2/g.[29]

Other routes such as dealumination[30] or desilication[11] also represent multistep procedures requiring several calcination and etching steps. A recent method by Perez-Ramirez et al.[31] relies on dealumination of only partially detemplated zeolites, which afforded control over the depletion range in the crystals and increased the total pore volume of micrometer-sized beta to 0.4 mL/g without decreasing the micropore volume (here 0.20 mL/g). Similar results were obtained by Holm et al. who used TMAOH for basic leaching,[14] resulting in surface areas of about 700 m^2.

The creation of mesoporosity can also be envisioned through the assembly of nanosized beta crystals. To prevent particle growth during the assembly, Serrano et al. have used a silanization method where a nanozeolite beta suspension was refluxed with TEAOH and different organosilane compounds. A second prolonged hydrothermal treatment was reported to give aggregates with a large surface area of up to 855 m^2/g and unusually large micropore volumes up to 0.345 mL/g. Unfortunately, the mesopore volume of the small mesopores was not given.[32,33] An interesting alternative route toward nanobeta-assemblies was reported recently by the group of Ryoo et al., using new cyclic diammonium cations as templates that contain phenyl or diphenyl spacers between the ammonium centers. These structure-directing agents (SDAs) appeared to preorganize the beta precursor gel through instantaneous gelation and afforded a pseudomorphic crystallization. Aggregates of about 20 nm crystallites resulted in a high mesopore volume (0.84 mL/g) and micropore volume (0.17 mL/g) with a BET surface area of 653 m^2/g.[34,35]

In our quest for hierarchical mesoporous zeolite beta, we explore the possibility of creating mesoporous spaces with similarly sized nanozeolites acting as "bricks". As a high concentration of nanozeolites appears to be conducive for such assembly, we focused our attention on the steam-assisted conversion of concentrated, nearly dry gels. Matsukata et al.[36−39] have applied the steam assisted conversion (SAC) method to the synthesis of zeolite beta. This method requires lower amounts of water and organic template than in conventional approaches and broadens the range of accessible Si/Al ratios from 7 to purely siliceous beta zeolites. It was developed on the basis of a method introduced by Xu et al.,[40] who reacted a previously formed ZSM-5 precursor gel via the vapor phase with an aqueous solution of the template; this was later named the dry gel conversion method (DGC). In the SAC method, the volatile phase consists solely of the solvent, usually water, while the remaining ingredients including the structure-directing agent or template (SDA) are mixed and subsequently dried to result in the precursor powder. The solvent necessary for conversion is kept separate from the solids in the autoclave during reaction.

Matsukata et al. have shown that the SAC method is very efficient for producing zeolite beta. Under optimal conditions with a low Si/Al ratio of about 15, they achieved a complete conversion in only 3 h at 180 °C when using colloidal silica as a precursor, resulting in a surface area of 600 m^2/g.[41] SEM investigations showed particle sizes between 180 and 400 nm with increasing silica content.[42] However, the nanoscale texture and mesoporosity of these materials were not reported. Some of us have recently demonstrated that the SAC method can be applied to synthesize mesoporous zeolite beta.[43] When micrometer-sized silica precursor grains were soaked with TEAOH and steamed at 150 °C for several days, the grains were transformed into self-sustaining beta aggregates, forming a secondary pore structure of about 10 nm diameter.

Here, we report an effective synthesis procedure for hierarchical mesoporous zeolite beta that is based on the common structure-directing agent TEAOH and that affords mesopores through controlled intergrowth of nanosized crystallites into an open network without using a second porogen. We find that an alkali-containing dense precursor gel can easily be converted in only a few hours into hierarchical zeolite beta materials in a one-step procedure. We use highly concentrated precursor gels and apply steam-assisted conversion to induce a burst in nucleation rate that yields completely crystalline and highly porous materials at different scales. It is demonstrated that the mesoporosity is caused by the assembly of extremely small and uniformly sized crystalline beta particles whose growth is arrested by the dense packing in the gel. During steam conversion these nanoparticles condense into a porous network characterized by very high surface areas. The synthesis of the nanozeolite assemblies was performed with Si/Al ratios between 10 and 33 using different silica precursor materials. The transformation of the silica

Table 1. Sample Compositions and Reaction Conditions

sample	Si/Al_{th}	Si/Al_{ICP}	reaction temperature T (°C)	duration of reaction (h)	sample amount (g)	saturation (X)
MB22-15-72	22	19.1	150	72	1	4
MB22-18-2	22		180	2	0.5	1
MB22-18-7	22	19.0	180	7	0.5	1
MB33-15-6	33		150	6	1	4
MB33-15-20	33		150	20	1	4
MB33-15-48	33	27.2	150	48	1	4
MB15-15-72	15	11.8	150	72	5	2
MB15-15-24[a]	15	12.1	150	24	2	4
MB10-12-120[a]	10	8.8	120	120	2	10
MB22-17-6-2	22	18.3	170	6	4	2
MB22-17-6-6	22	18.5	170	6	4	6

[a] TEAOH was increased from 1:0.425 to 1:0.64 with respect to SiO_2.

precursor into hierarchical zeolitic materials was followed with nitrogen sorption, mercury intrusion porosimetry, scanning and transmission electron microscopy (SEM and TEM), and dynamic light scattering (DLS). We also demonstrate that the amount of water used for the steam treatment is critical for the growth kinetics. With optimized conditions, it is possible to obtain mesoporous zeolite beta with high micro- and mesoporosity in a highly efficient single step procedure.

EXPERIMENTAL SECTION

Sample Preparation. The synthesis was performed with sodium hydroxide NaOH 97%; aluminum sulfate $Al_2(SO_4)_3 \cdot 18\ H_2O$, Aldrich; tetraethyl ammonium hydroxide,TEAOH, 35% aqueous solution, BASF; mesoporous silica (Si415) ACROS 40−60 μm, 270 m^2/g, 15 nm pores (used as standard silica precursor; other mesoporous silica materials used differ in grain size, mesopore size, and surface area, as described in the text). Fumed silica (CAB-O-SIL, 380 m^2/g) can also be used instead of mesoporous silica, resulting in similar textural properties.

Standard molar reactant ratios for an Si/Al ratio of 22 were as follows: $1SiO_2$:$0.023Al_2O_3$:0.049NaOH:0.425TEAOH:$6.8H_2O$.

The reaction was carried out in the following way, serving as an example: 0.066 g of NaOH, 0.507 g of $Al_2(SO_4)_3 \cdot 18H_2O$, and 6 g of 35% aqueous TEAOH were mixed and stirred until clear (15−30 min). Next, 2.0 g of silica was added, and the mixture was further stirred for about 1 h, resulting in a viscous gel that was heated at 60 °C to complete dryness. The resulting dry precursor lumps were coarsely crushed and transferred into a 4 mL Teflon cup, which itself was placed into a 20 mL Teflon liner. The amount of 0.1−0.495 mL water was added into the bottom of the liner without contacting the dry gel in the inner Teflon cup (the amount of water was adjusted according to temperature and reactor volume to result in a multiple of the amount necessary to reach a steam-saturated atmosphere, termed X in the following text). The charged liner assembly was placed into a 20 mL steel reactor and transferred into a preheated oven at the desired reaction temperature (usually 180 °C, down to 120 °C) and heated for a period between 2 h and 3 days as described in the text, and the reaction was subsequently quenched. The converted gel was washed by filtration and dried. Template removal was performed by calcination in air with a temperature profile of 2 °C/min to 550 °C, where the sample was kept for 6 h. Elemental analysis of the calcined samples resulted in Si/Al ratios close to the theoretical values as mentioned in the text. Colloidal solutions were purified by 3-fold centrifugation in water at 20 000 rpm (47 800g) for at least 45 min.

The final yield relates to the solid amounts retrieved after calcination in comparison to the amounts of silica and alumina in the reaction gel. "Near 100 %" indicates a retrieval of about 95% of the calculated amount, where up to about 5% may be lost due to handling.

Characterization. X-ray diffraction data were collected on a STOE powder diffractometer in transmission geometry with Cu $K\alpha_1$ (λ = 1.5406 Å). SEM micrographs of uncoated powders immobilized on sample holders with silver paste were obtained on the field emission microscope JEOL JSM-6500F, using 4 keV. Transmission electron microscopy was performed with a JEOL 200 kV TEM. Zeolite powder was immersed in ethanol, sonicated, and one to two drops were spread on copper grids covered with holey carbon.

Nitrogen sorption isotherms at −196 °C were measured on previously evacuated samples (at 150 °C overnight) using a Quantachrome Nova 4000e. Micropore volumes were determined from t-plots in the range between 0.12 and 0.5 P/P_0 (de Boer). The apparent surface areas were determined with the Brunauer−Emmett−Teller (BET) model in the range between P/P_0 0.02−0.16. The total pore volume was evaluated at P/P_0 = 0.99. Pore size calculations were performed with the NLDFT method based on the desorption isotherms, using the nitrogen on silica, cylindrical pore NLDFT equilibrium kernel, and compared to results obtained from the adsorption branch as mentioned in the text. Mercury intrusion porosimetry was used to determine meso- and macropore size distributions between 3 nm and 300 μm with a Micromeritics Autopore IV 9520 mercury intrusion porosimeter. Dynamic light scattering (DLS) was measured on a Malvern Zetasizer Nano ZS in aqueous solutions in 1.5 mL PMMA cuvettes. Raman spectra were recorded on powdered samples with a Jobin Yvon Horiba LabRam-HR800 Raman microscope equipped with a 632.8 nm HeNe laser. Thermogravimetric measurements were performed on a Netzsch STA 440 C Jupiter TG/DSC instrument with a heating rate of 10 °C/min in synthetic air. Chemical analysis of the samples was performed by inductively coupled plasma atomic emission spectroscopy (ICP-AES). The sample compositions and reaction conditions are listed in Table 1. Sample names of the mesoporous beta (MB) zeolites include the Si/Al ratio, temperature, and duration in hours. For example, MB22-15-72 refers to a mesoporous beta with an Si/Al ratio of 22 that was synthesized at 150 °C for 72 h.

RESULTS AND DISCUSSION

Mesoporous Zeolite Beta with Medium Aluminum Content: Si/Al = 22. The concept of using nanozeolites as building blocks in the assembly of hierarchical zeolitic materials requires a synthesis method that favors high nucleation rates. This is achieved via highly concentrated gels that are processed using the steam-assisted conversion (SAC) method. Previous studies in our group have shown that mesoporous zeolite beta can be obtained

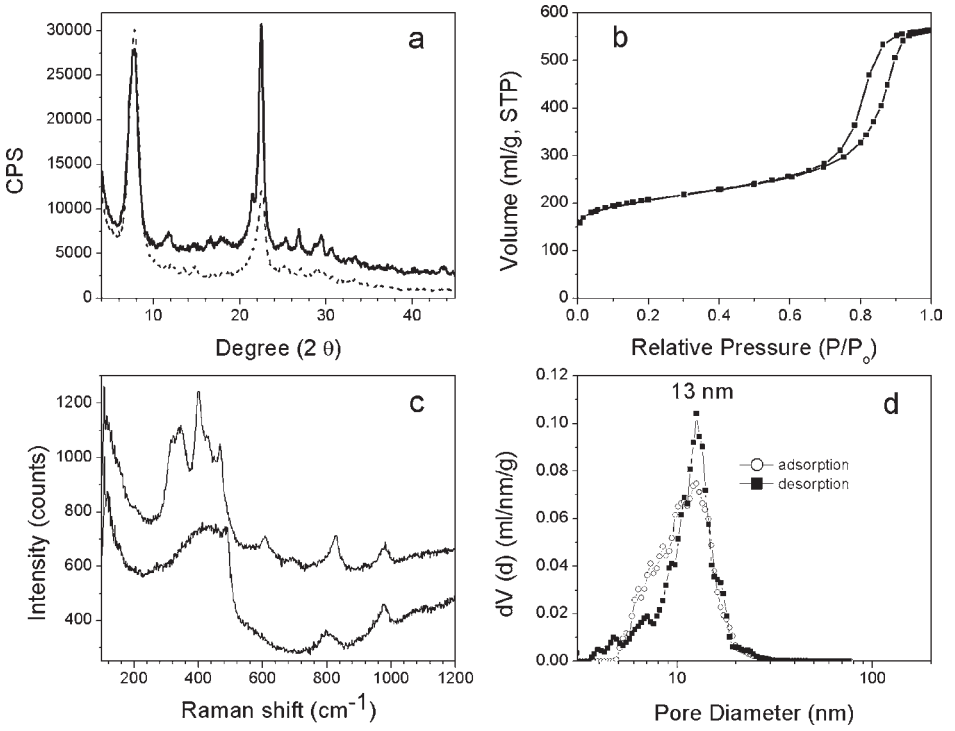

Figure 1. Characterization of sample MB22-15-72, reacted at 150 °C for 3 days: (a) XRD of uncalcined (thick line) and calcined sample (dotted line), (b) nitrogen sorption isotherm and (d) corresponding pore size distributions (NLDFT method) as derived from the adsorption and desorption branch, and (c) Raman spectrum of MB22-15-72 (top) and amorphous silica (bottom).

by the SAC method at 150 °C when the dried precursor gels were reacted for about 5 days.[43] Here, we have changed the preparation of the precursor gel and varied the reaction conditions to allow for a faster conversion into crystalline zeolite beta. With molar ratios of $1SiO_2$:$0.023Al_2O_3$:0.049NaOH:0.425TEAOH:$6.8H_2O$, we have added a small amount of sodium hydroxide to the impregnating solution and we use less structure-directing agent in a denser gel. Alkali cations are usually strictly avoided in the synthesis of colloidal zeolites because they accelerate the agglomeration of nanoparticles. Here, however, this effect is desired. Further, we use aluminum sulfate as an aluminum source that is easily dissolved under our conditions and is believed to be a crystallization promotor.[44] After all ingredients were mixed, the gel was dried at an elevated temperature of 60 °C. Under these conditions, we were able to produce highly mesoporous zeolite beta already after 3 days at 150 °C. Following the SAC treatment, self-supporting grains with a glassy appearance could easily be recovered by filtration (MB22-15-72). Figure 1a displays the strong X-ray diffraction intensities of zeolite beta before and after calcination, showing no trace of an amorphous background indicative for unreacted silica. Furthermore, the Raman spectrum of the calcined sample in Figure 1c, top, displays only modes of a fully condensed lattice that are assigned to five-membered rings (324 and 344 cm^{-1}), six-membered rings (400 and 428 cm^{-1}), and four-membered rings (468 cm^{-1})[45] without indication of the broader feature of amorphous silica at 490 cm^{-1} (Figure 1c, bottom).

Nitrogen sorption shows a typical type IV isotherm for mesoporous solids. Its evaluation further illustrates the complete conversion of the precursor into highly crystalline beta by showing a large micropore volume of 0.214 mL/g (t-plot, see Table 2). The highest values for micropore volumes are found in large single crystals of zeolite beta (up to 0.23 mL/g for 14 μm-sized pure silica beta[46]), but usually micropore volumes of 0.19 mL/g and lower are reported for small crystallites.[47] Thus, a high value as found for the above sample MB22-15-72 indicates the complete absence of unconverted mesoporous silica from the precursor slabs, especially because the latter do not show any significant microporosity (0.01 mL/g). Strikingly, the isotherm shows a strong increase at higher relative pressures, pointing to large textural mesoporosity. Indeed, an unusually high BET surface area of 751 m^2/g was measured, which is comparable to or larger than that of extremely small discrete zeolite beta nanoparticles.[43,47,48] Similar to sorption in a bed of nanoparticles, we observe a large hysteresis in these zeolite beta grains between the adsorption and desorption branch. Figure 1d shows a dominant pore diameter of 13 nm of this secondary pore system when analyzed with the NLDFT method. We notice that the pore size distribution obtained from the adsorption branch is nearly identical to that from the desorption branch, showing that the hysteresis originates solely from delayed nitrogen condensation. Pore blocking or percolation effects seem not to be present. It can therefore be regarded as a type H1 hysteresis, which is only found in well-defined cylindrical pores or in material agglomerates consisting of extremely uniform particles.[49] To our knowledge, similar well-defined pore systems have not been reported for hierarchical zeolite beta. The total pore volume of sample MB22-15-72 at $P/P_0 = 0.99$ was determined to be 0.867 mL/g. Again, comparable total pore volumes have usually only been obtained for beds of zeolite beta powder having domains of about 30 nm made by hydrothermal synthesis with highly diluted gels but frequently at a significant reduction of microporosity, for example, only 0.099 mL/g.[50]

Scanning and transmission electron microscopy was used to elucidate the nanoscale morphology of the zeolitic material. The morphology of the precursor silica particles before and after SAC

Table 2. Nitrogen Sorption Data and Hg-Intrusion Results for Selected Samples

sample	BET surface area (m^2/g)	μ-pore volume (t-plot) (mL/g)	total pore volume $(mL/g)_{0.99}$	pore diameter (N_2, NLDFT) (nm)	pore diameter (Hg-intrusion) (nm)
MB22-15-72	751	0.214	0.867	13	
MB22-18-2	631	0.208	0.745	8−30	
MB22-18-7	717	0.225	0.939	14	
MB33-15-6	587	0.112	0.463	4.5 + 10	
MB33-15-20	574	0.149	0.512	4.3 + 20	
MB33-15-48	763	0.223	0.833	12	4−14
MB15-15-72	690	0.217	0.887	3−30	20−250
MB15-15-24[a]	686	0.171	0.993	13	4−50
MB10-12-120[a]	676	0.174	0.985	4.4 + 8−32	
MB22-17-6-2	493	0.090	0.753	9 + 13	
MB22-17-6-6	714	0.203	0.902	13	

[a] TEAOH was increased from 1:0.425 to 0.64 with respect to Si.

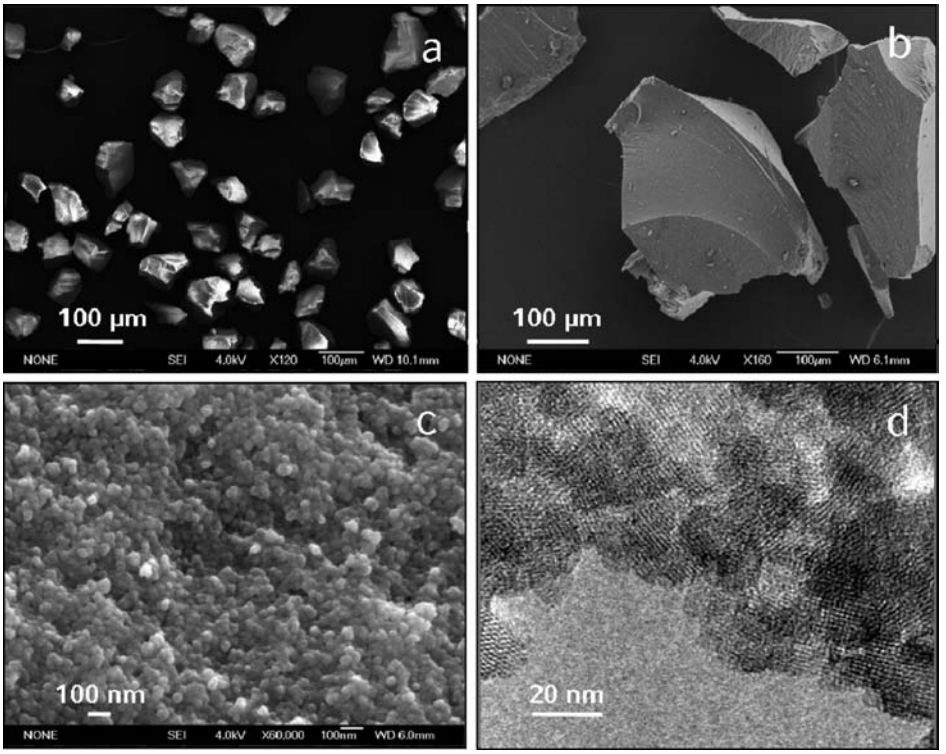

Figure 2. (a) Precursor silica Si415, (b) self-sustaining hierarchical zeolite pieces after SAC treatment of sample MB22-15-72, (c) surface of particles in (b) with higher resolution, and (d) TEM of sample MB22-15-72.

treatment is shown in Figure 2a and b−d, respectively. The original silica precursor particles are about 50−100 μm in size. After steam treatment and conversion into zeolite beta, we observed a profound transformation into much larger pieces. The seemingly smooth surface at low magnification (Figure 2b) turns out to be composed of very small zeolite beta particles when imaged at higher magnification (Figure 2c). It shows aggregated particles that are modulated into a surface with macro- and mesopores, giving rise to the large pore volume observed with nitrogen sorption.

Analysis with high-resolution electron microscopy reveals that the particles are completely crystalline throughout the sample as substantiated by lattice fringes all over the specimen. Individual particles can be recognized with sizes in the range of 20 nm, thus consisting of only about 10 unit cells in each dimension, and causing the extremely large surface area. The effective intergrowth of the individual grains gives rise to the substantial mesoporosity. In some areas, it is possible to recognize lattice fringes extending over several particles, indicating an oriented assembly/growth over greater distances. This might explain the relatively narrow reflections with high intensity in the XRD patterns. Nanozeolites usually show a broadening and decrease in peak height. We emphasize that the yield of these hierarchical zeolite beta assemblies is nearly 100%, in stark contrast to the low yields (often less than 10%) of nano particles usually obtained from clear solutions.[51]

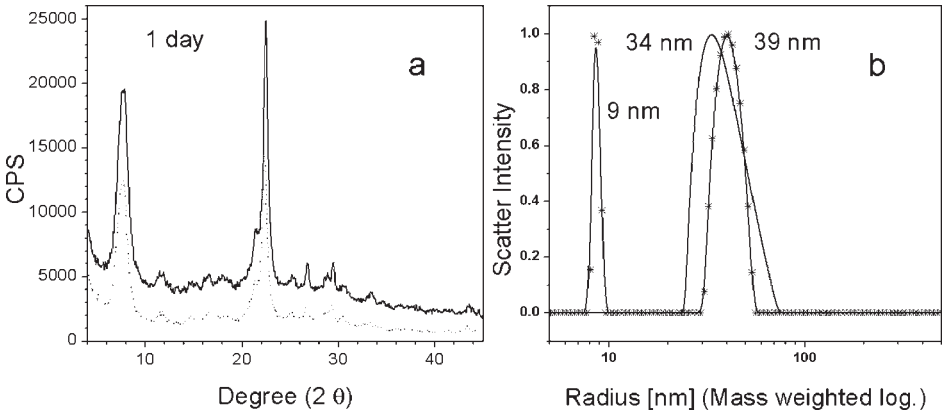

Figure 3. (a) XRD of uncalcined sample MB22-15, Si/Al = 22, at 150 °C after 1 day, solid fraction (dark line) and colloidal fraction (dotted line); and (b) DLS of colloidal fraction: after 1 day (symbols) and after 2 days (straight line) of reaction.

Evolution of the Hierarchical Zeolite Structure with Reaction Time. We have investigated the synthesis procedure at the temperature of 150 °C at different time intervals to elucidate the evolution of the hierarchical zeolite materials. Two 20 mL reactors were each filled with 1 g of the same precursor gel and removed from the oven after 1 and 2 days, respectively. Both samples exhibited a turbid filtrate upon washing, containing a colloidal solution in addition to a solid powder. The filtrate was collected and further isolated by high speed centrifugation. The solid cake was redispersed twice by sonication and again centrifuged. The resulting transparent gels were dried after the final washing process and analyzed by X-ray diffraction. The corresponding diagrams of the solid and the colloidal fraction after 1 day of reaction are compared in Figure 3a. It shows that both samples contain highly crystalline zeolite beta. Crystallization is obviously completed even after 1 day; however, assembly/intergrowth into self-sustaining monolithic particles is not finished at that time. Similar results were obtained for the sample after 2 days of reaction.

The assessment of the retrieved amounts of the solid and colloidal fraction showed the following trend: the solid yield increased from 60% after 1 day to 73% after 2 days, to finally close to 100% after 3 days. The colloidal fraction decreased accordingly from 40% after 1 day to 35% after 2 days, while after 3 days at 150 °C the filtrate was completely clear. The particle size of the colloidal fraction was analyzed with dynamic light scattering, shown in Figure 3b. Two different populations with particle diameters of about 18 and 68 nm were measured after 1 day, while agglomeration of the smaller particles into about 80 nm colloids is observed after 2 days. We note that when a classical hydrothermal reaction was performed on these concentrated gel mixtures with a water content similar to that used for the SAC conversion, it resulted in a purely colloidal solution after 3 days at 150 °C. Here, particles with a diameter of about 130 nm and a smaller BET surface area of 680 m^2/g were obtained, at a yield of about 75% (not shown).

The reaction procedure as described above gives very reproducible results even when larger amounts of sample are treated under SAC conditions. Similar surface areas between 744 and 760 m^2/g with large mesoporosity were measured with up to 16 g of dry gel in a 100 mL autoclave, when the added amount of water was accordingly increased to 0.5 mL to result in the same degree of steam saturation. The procedure is also applicable to other silica precursors. Four different silica precursors with differing grain sizes from 0.2 (Cabosil) to 60−200 μm in size (ACROS) and mesopores from 4 to 15 nm (and different surface areas from about 500 to 270 m^2/g) were treated under similar reaction conditions of 3 days at 150 °C. All gave very comparable results.

In our previous report,[43] it was observed that increasing the reaction temperature to 170 °C led to phases other than zeolite beta. For instance, a mixture of beta and MTW was formed after 3 days. The formation of hierarchical zeolite materials as described here is characterized by an accelerated conversion into zeolite beta. This suggests that the nucleation rate to zeolite beta is strongly enhanced under our optimized conditions, thus possibly allowing us to perform the reaction at a higher temperature in a shorter period of time, and suppressing the formation of a foreign phase. Reactions were therefore performed at 180 °C, and the development of the zeolite materials was studied. Remarkably, zeolite beta was formed under these conditions after only 2 h as seen in Figure 4a, showing an XRD intensity similar to that in Figure 1a after 3 days at 150 °C.

Further, no significant changes were observed when performing the reaction for up to 7 h at 180 °C. However, comparative nitrogen sorption measurements give an indication for a slight residue of amorphous gel in the sample reacted for only 2 h: while the short reaction time results in only 631 m^2/g surface area, the longer time of 7 h yields a surface area of 717 m^2/g, concomitant with an increase in micro- and mesopore volume (sample MB22-18-7; see Table 2). However, even after this prolonged time at elevated temperature, there is no recognizable change in particle size as is shown in Figure 4b.

Mesoporous Zeolite Beta with Low Aluminum Content: Si/Al = 33. The efficiency of the synthesis of hierarchical zeolite beta with medium aluminum content led us to broaden our study to different Si/Al ratios. Changing the ratio from about 22 to 33 reduces the Al content per unit cell with $Al_xSi_{64-x}O_{128}$ from about 3 to 2, thus increasing the amount of TEA^+ relative to AlO_4^- markedly under our standard reaction conditions. When the synthesis was performed at 150 °C and followed in time, we could observe a conversion into solid, retrievable zeolite beta already after 6 h. Similar to the results with an Si/Al ratio of 22, the conversion into a solid beta phase was still incomplete at this stage (ca. 50%) and accompanied by a larger fraction of colloidal zeolite suspension. Zeolite beta nanoparticles were still observed after 20 h, but 48 h was sufficient for a 100% conversion into solid hierarchical beta aggregates (in contrast to 72 h required with an Si/Al ratio of 22). However, when the X-ray diffraction data were

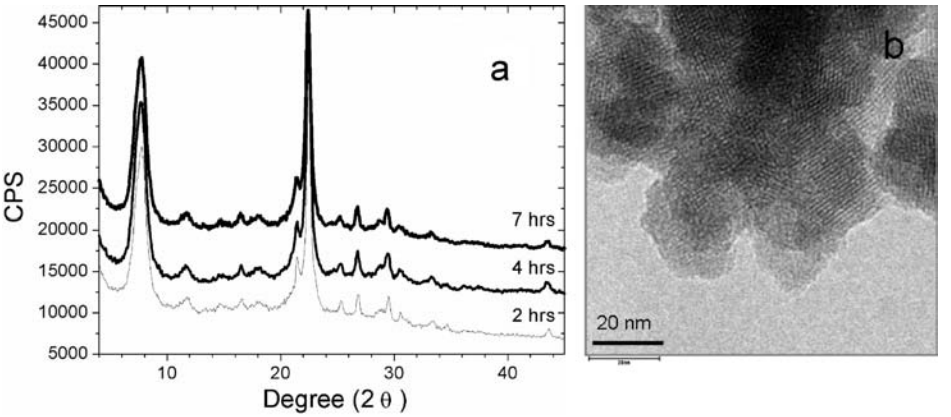

Figure 4. (a) XRD patterns of sample MB22-18, Si/Al = 22, at 180 °C after 2, 4, and 7 h (raw data are stacked), and (b) TEM of sample MB22-18-7 after 7 h, uncalcined.

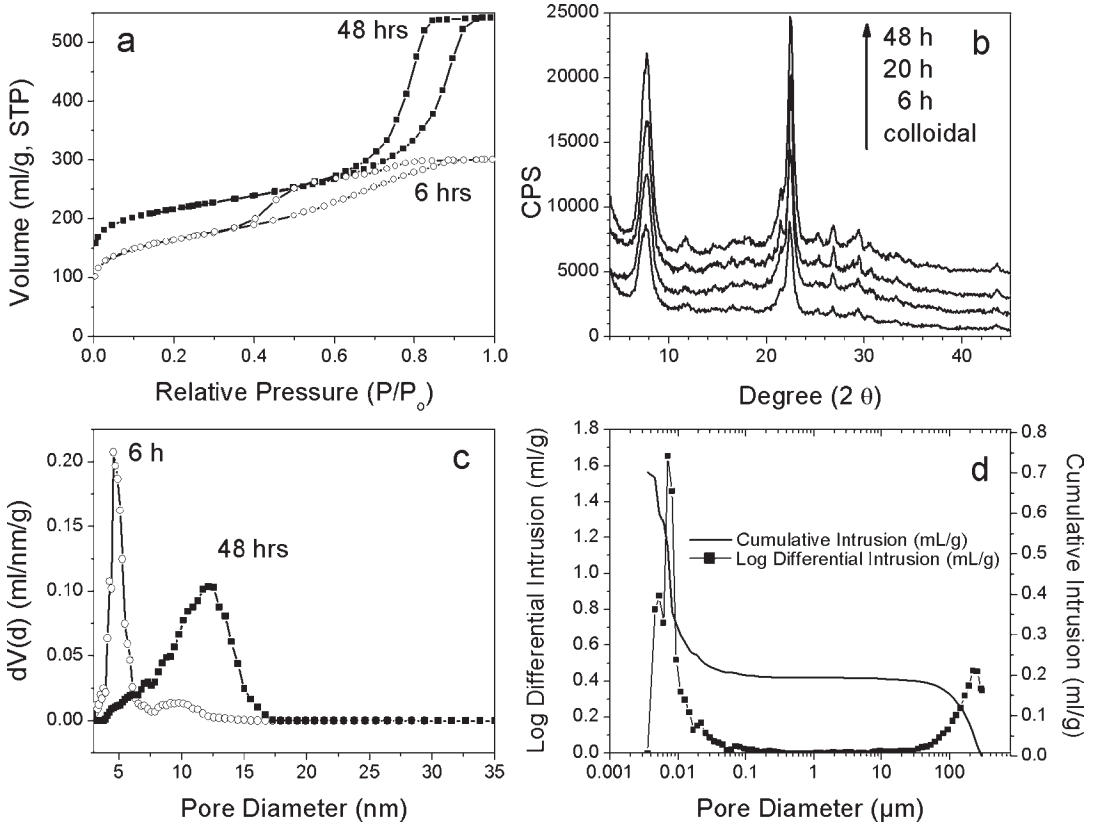

Figure 5. Development of sample MB33-15 heated at 150 °C, Si/Al = 33: (a) nitrogen sorption isotherms of samples heated for 6 h (○) and 48 h (■) at 150 °C, (b) X-ray diffraction patterns of uncalcined samples (stacked), (c) NLDFT pore-size distributions, and (d) mercury intrusion porosimetry of sample MB33-15-48.

carefully analyzed, a slight increase in the baseline of the solid samples could be seen after 6 and 20 h in comparison to the straight background in the colloidal samples, thus indicating the presence of a small amorphous residue (see Figure 5b). Nitrogen sorption data of the retrieved solids after these shorter reaction times confirmed that the silica grains were not fully transformed into zeolite beta in less than 48 h. Figure 5a shows a notable microporosity already after 6 h; however, it grows further when heating for 48 h.

Obviously, the restructuring of the silica precursor into microporous material had already started after 6 h, but the microporosity of only 0.112 mL/g (t-plot) after 6 h in contrast to 0.223 mL/g after 48 h shows that some part of the solid is still amorphous (sample MB33-15-6; see Table 2). This incomplete restructuring of the silica precursor is also reflected in the hysteresis, indicating tortuosity after 6 h of reaction. The original porosity of the precursor silica with 11.5 nm pore diameter and a large pore volume of 1.256 mL/g has collapsed, and a peak at 4 nm is predominant when the desorption branch is analyzed (see Figure 5c). Similar peaks were always observed when the conversion into zeolite beta was not completed, and this peak in the pore-size distribution curve is believed to be an artifact. It likely results from supercritical nitrogen desorption caused by

dx.doi.org/10.1021/ja108698s |J. Am. Chem. Soc. 2011, 133, 5284–5295

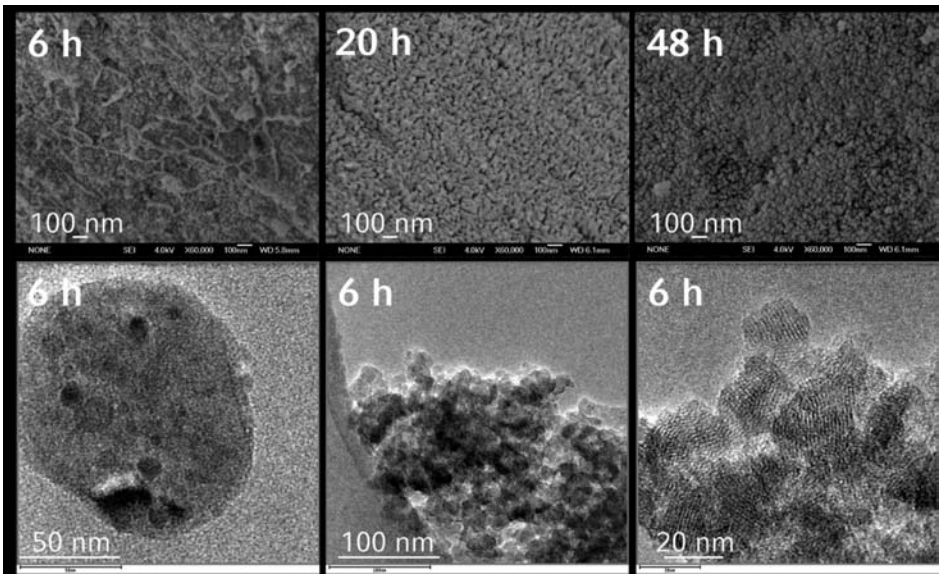

Figure 6. Sample MB33-15, Si/Al = 33: top row, SEM of samples reacted for 6, 20, and 48 h at 150 °C (scale bar 100 nm); bottom row, TEM of different regions in sample MB33-15-6 after 6 h of reaction.

diffusion limitations in a disordered pore network.[49] This peak vanishes as soon as the precursor is completely transformed into zeolite particles after 48 h, showing truly hierarchical zeolite beta materials (MB33-15-48). A plateau in the desorption curve of the isotherm at high pressure again indicates well-defined mesopores. An average pore diameter of 12 nm is calculated with the NLDFT approach. Hg-intrusion measurements confirmed the narrow mesopore range, detecting pores between 4 and 14 nm. No larger meso- or macropores are observed up to 300 μm (see Figure 5d). It should be noted that the mesopore volumes determined by nitrogen sorption (total pore volume minus micropore volume) are close to the total intrusion volume determined from mercury porosimetry (3 nm to 1 μm pore size). For example, in sample MB33-15-48, the mesopore volume determined from nitrogen sorption is 0.61 mL/g, similar to 0.51 mL/g determined by Hg-intrusion measurements.

The rearrangement in the mesopore architecture, as seen in Figure 5a in the evolving samples, indicates a high local mobility of aluminosilicate building blocks during the synthesis of zeolite beta even in these "dry" gels under SAC conditions. DLS mesurements and SEM analysis (see below) suggest that the initial transformation into nanosized particles starts at the surface of the silica precursor. SEM pictures of the sample after 6 h reaction time show a distinct roughening of the surface (Figure 6). Very small particles of 10−20 nm are partially aligned into a net of strings covering the individual grains. They probably form the nanoparticles that can be collected when the sample is washed at this stage. These protrusions on the exterior start to smooth out upon increasing reaction time and increasing crystallite formation. A rather homogeneous morphology of evenly distributed, tightly packed particles of about 20−30 nm diameter is observed upon full conversion after 48 h. Corresponding transmission electron micrographs of the 6 h sample show the simultaneous appearance of highly crystalline aggregated particles (in Figure 6b, middle and right), as well as apparently amorphous residues on the left. Darker areas in the amorphous region (Figure 6b, left) might indicate density fluctuations as starting points for crystallization.

Mesoporous Zeolite Beta with High Aluminum Content: Si/Al = 15 to 10. The SAC procedure was further applied to precursor gels with lower Si/Al ratios using the "standard" conditions. When the reaction was performed at 150 °C for 24 h with an Si/Al ratio of 15, all of the sample was retrieved as solid and no nanoparticles were observed, unlike the situation with an Si/Al ratio of 22 or 33. However, X-ray diffraction still showed a small but significant amorphous background in the zeolite beta diffraction pattern. On the other hand, prolonging the reaction time again to 3 days resulted in a sample with an X-ray diffractogram showing high intensities (MB15-15-72). Further, the nitrogen sorption isotherm of this sample was nearly flat over the pressure range between 0.05 and 0.8 P/P_0 (see Figure 7e). Such results are characteristic for zeolite beta powders consisting of larger crystallites. SEM analysis confirmed this conclusion. The silica precursor was completely transformed into macroscopic pieces assembled of particles sized about 150 nm instead of 20−30 nm (see Figure 7a,c). The higher aluminum content in this sample apparently accelerated the conversion into zeolite beta and induced zeolite crystal growth already after 3 days. To shorten the induction period and stimulate nucleation, we increased the SDA concentration in the impregnating solution from 0.425 to 0.640 mol of TEAOH per mol of SiO_2 (sample MB15-15-24*). A complete conversion into zeolite beta was now achieved within only 1 day at 150 °C, simultaneously showing a profound effect on particle size and mesoporosity. A comparison between both samples is displayed in Figure 7.

The SEM reveals now again a particle size of not more than about 30 nm after increasing the template concentration, and nitrogen sorption accordingly shows a higher surface area and an apparently larger mesoporosity (MB15-15-24*; see Table 2, Figure 7b,d,e). The total pore volume increased from 0.887 to 0.993 mL/g for these two samples. Sample MB15-15-24* shows a well-defined pore-size maximum of 13 nm (Figure 7f, determined via nitrogen sorption). Complementary mercury intrusion experiments enable the detection of larger pores. The corresponding results of these two samples are displayed on the bottom of Figure 7(g,h). Figure 7g shows that the larger beta crystals of

dx.doi.org/10.1021/ja108698s |*J. Am. Chem. Soc.* 2011, 133, 5284–5295

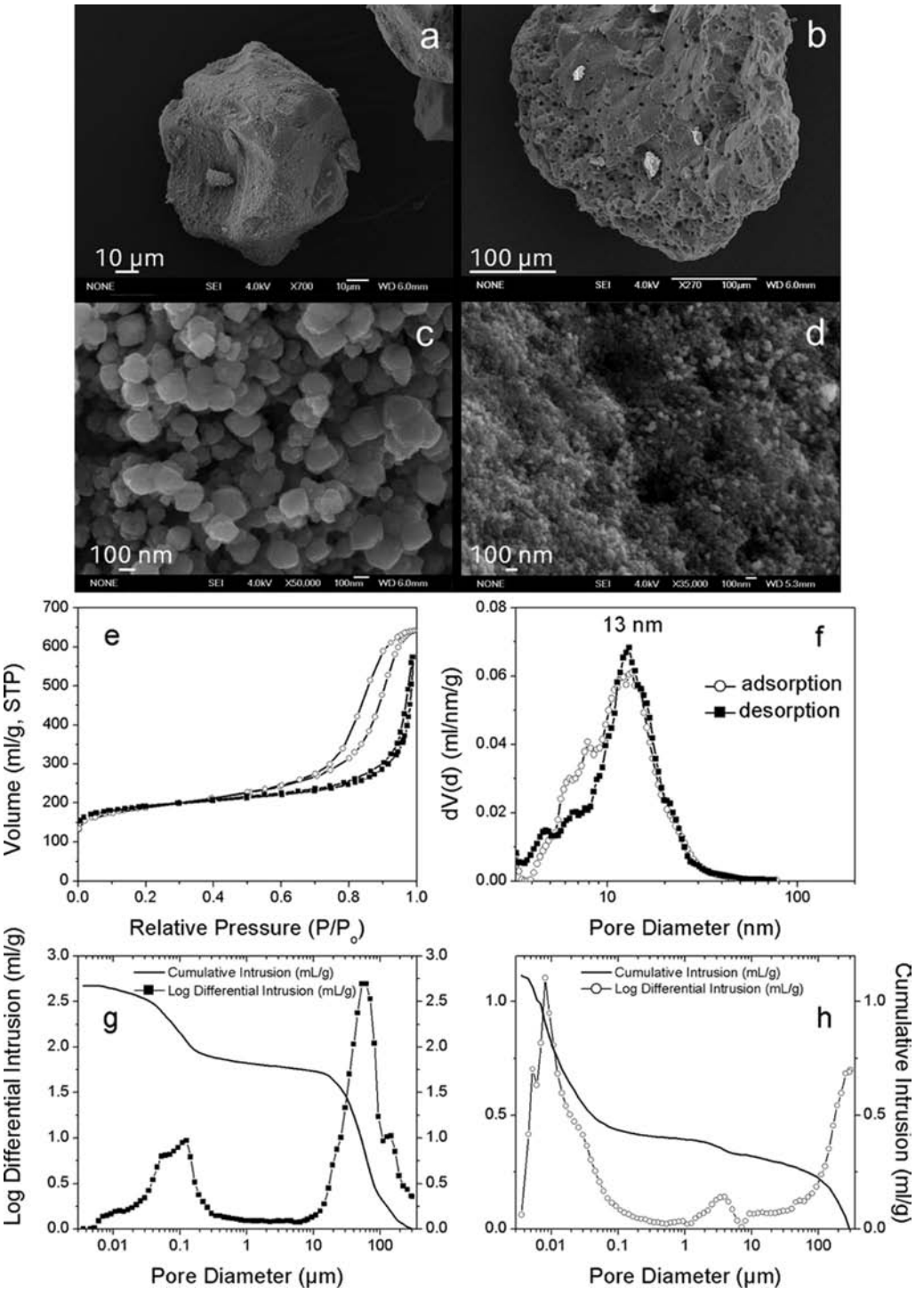

Figure 7. (a,c) SEM image of sample MB15-15-72, Si/Al = 15, TEAOH 0.425, reacted at 150 °C for 3 days; (b,d) SEM image of sample MB15-15-24*, Si/Al = 15, TEAOH 0.64, reacted at 150 °C for 1 day; scale bars are shown in the figures; (e) nitrogen sorption of samples MB15-15-72 (●) and MB15-15-24* (○); (f) pore size distribution of sample MB15-15-24* as derived from the adsorption and desorption branch (NLDFT method); (g) Hg-porosimetry of MB15-15-72; and (h) Hg-porosimetry of MB15-15-24*.

about 150 nm in sample MB15-15-72 have created interparticle voids ranging between 20 and 250 nm diameter, which extends beyond the detection range of nitrogen sorption. Consequently, the mesopore volume of 0.853 mL/g from Hg-porosimetry is higher than that detected by nitrogen sorption (0.67 mL/g). A second peak at about 50 μm diameter originates from spaces between the large zeolite beta pieces, as displayed in Figure 7a. On the other hand, sample MB15-15-24* (Figure 7h), consisting of much smaller 30 nm beta crystals, displays accordingly also much smaller mesopores, ranging between 4 and 50 nm. The macropores resulting from spaces between the beta pieces (Figure 7b) are larger than 100 μm. Here, we find similar mesopore volumes when determined by nitrogen sorption (0.822 mL/g) and mercury intrusion measurements (0.723 mL/g up to 1 μm pores).

dx.doi.org/10.1021/ja108698s |*J. Am. Chem. Soc.* 2011, 133, 5284–5295

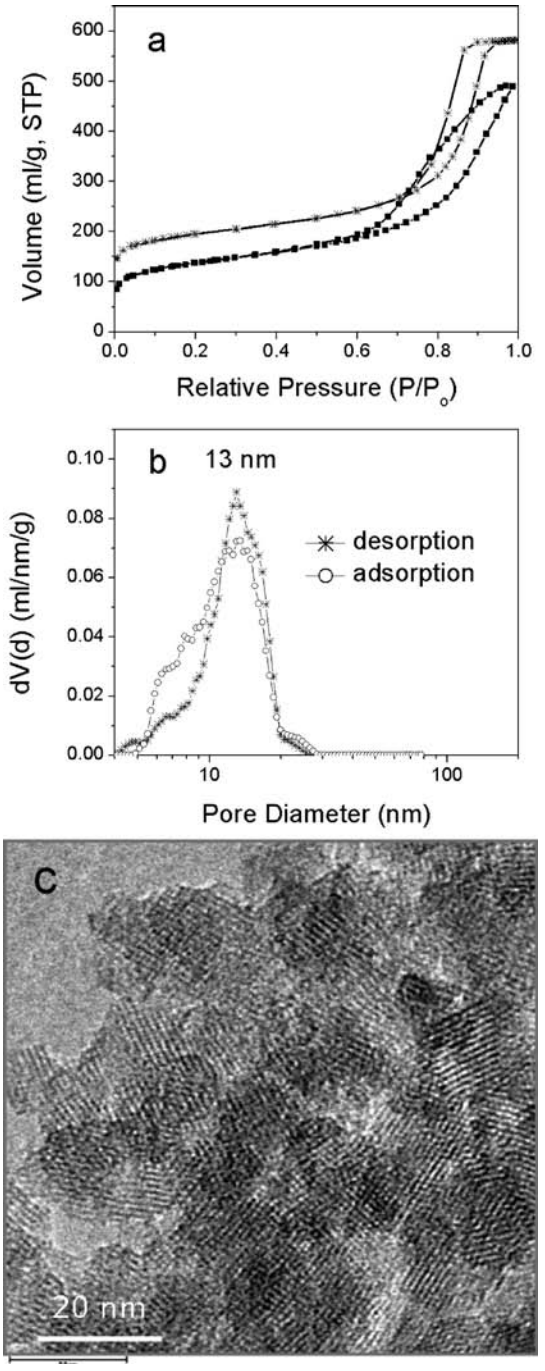

Figure 8. SAC conversion at 170 °C for 6 h: (a) nitrogen sorption isotherms of sample MB22-17-6-2 with 4 g of gel and X2 water amount (■), and sample MB22-17-6-6 with 4 g of gel and X6 amount of water (*), (b) pore-size distribution of sample MB22-17-6-6 as derived from the adsorption and desorption branch (NLDFT method), and (c) electron micrograph of the 130 g sample, X6 amount of water, calcined.

These examples demonstrate that the size of the mesopores is primarily determined by the size of the individual zeolite nanocrystals that are tightly intergrown through the SAC synthesis approach. Furthermore, it nicely illustrates that changing the particle size of the constituting zeolite crystals is a means for tuning the mesopore volume and size.

When the Si/Al ratio was further decreased to 10, an additional adjustment of the reaction conditions had to be made. In this case, even with a higher concentration of 0.64 mol of TEAOH, it was not possible to obtain a complete conversion at 150 °C after 3 days of reaction. However, when the reaction temperature was lowered to 120 °C under otherwise exactly the same reaction conditions (including the absolute amount of water), we observed a higher degree of conversion within the same time period. Highly crystalline hierarchical zeolite beta materials were obtained after 5 days at this temperature (sample MB10-12-120*; see Table 2).

Impact of Water Concentration on Steam-Assisted Conversion. A prerequisite for the formation of hierarchical zeolite beta materials following the SAC approach is a high local concentration of aluminosilicate species in the gel, which is achieved by a low water concentration in the system. However, the in situ formation of water during the condensation reaction of silica or alumina alone is not sufficient to drive the crystallization. This was confirmed by heating a dry synthesis gel at reaction temperature for a prolonged time, as has been reported previously.[42] On the other hand, we observed a strong dependence of the degree of conversion and required reaction time on the amount of added water. Principally, steam saturation needs to be achieved: therefore, the amount of added water needs to be scaled with respect to temperature and reactor volume. The amount required for a saturated atmosphere is sufficient as long as small quantities of gel are converted (see Figure 4a: 0.5 g is converted at 180 °C in 2 h at simple saturation (X1) to yield zeolitic material with 631 m^2/g surface area). When larger batches were synthesized (e.g., 4 g), we observed that an optimum conversion was only achieved when the amount needed for saturation was increased by a factor of 6 (see Figure 8a, sample MB22-17-6-2 and sample MB22-17-6-6). A much higher conversion was possible under the latter conditions, resulting in hierarchical beta samples with 714 m^2/g (X6 the saturation amount) instead of 493 m^2/g (X2 the saturation amount). The well-defined type IV isotherm of the completely transformed sample MB22-17-6-6 shows again a good agreement between the pore-size distributions obtained from the adsorption and desorption branch. This demonstrates the formation of a homogeneous, hierarchical pore system even under these extreme reaction conditions (Figure 8b). The 6-fold saturation was found to be the optimum amount of water over a wide range of samples that were synthesized in different reactors of 20 mL (2 and 4 g of solids), 100 mL reactors (18 g), as well as 2000 mL reactors (130 g); these reactions were highly reproducible. Even the largest amount of 130 g obtained in the 2000 mL reactor still showed the extremely small aggregated nanoparticles of 10−20 nm (Figure 8c).

In view of these findings, we reasoned that the increased conversion of sample MB10-12-120 with an Si/Al ratio of 10 at the lower temperature of 120 °C could also be related to the amount of water present in the reactor. The same amount of 0.2 mL of water was added at 150 and 120 °C, which translates into an increase in water concentration relative to saturation from X4 to X10 at the lower temperature; that is, a larger relative amount of liquid water must exist under reaction conditions. This might induce a more open gel structure, allowing for greater mobility with respect to rearrangement in the gel and/or nutrient transport. Thus, it is reasonable to assume that the crystallization and intergrowth will be accelerated under these conditions, in comparison with the more restricted conditions of a denser gel. Indeed, reducing the amount of water at this temperature gave a lower conversion during the same reaction time.

This example demonstrates that it is possible to create hierarchical zeolite beta materials even with high alumina

Scheme 1. Formation of Hierarchical Zeolite Beta from a Dense Precursor Gel[a]

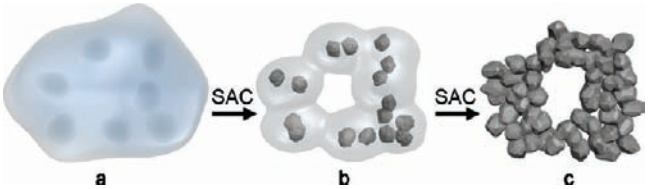

[a] (a) Dense precursor gel with concentration fluctuations leading to nucleation; (b) contraction (densification) and partial conversion of the gel into nanozeolites after short SAC treatment; at this stage, filtration yields a colloidal solution of zeolite beta; and (c) continued SAC reaction converts residual gel completely into small aggregated crystallites; the low mobility in the nearly dry environment arrests nanocrystals into a hierarchical zeolite network.

content, but that it is necessary to carefully adjust the experimental conditions for optimum results.

SUMMARY

In this study, we have demonstrated that with concentrated gel compositions and steam-assisted conversion, it is possible to create hierarchical zeolite beta materials without using an additional porogen and without the need for secondary processing. High conversion rates were achieved over a wide range of Si/Al ratios studied from 10 to 44. The zeolite materials obtained feature very high surface areas and micropore volumes, induced through the formation of extremely small primary zeolite crystallites with a narrow size distribution between only 10 and 20 nm. The final yield based on the aluminosilicate precursor is nearly 100%. We note that these mesoporous zeolite materials are resistant against mechanical or thermal treatments such as exposure to high intensity ultrasound or stirring in boiling water for several hours. The samples kept their integrity; all could easily be filtered after these treatments and did not disintegrate into nanozeolite suspensions. Nitrogen sorption measurements of the resulting samples did not show any marked changes in mesoporosity. The mesopore size distributions as well as the volume were nearly identical.

The suggested formation of zeolite beta nano crystallites and their arrangement into a hierarchical zeolite material is depicted in Scheme 1.

Here, mesopores are generated in a multistep process. Step a involves formation of numerous nucleation centers by using a dense dried precursor gel. Step b shows successive transformation of these nucleation sites into nanocrystallites, aided by the steam atmosphere at the beginning of the SAC reaction. This step includes a local rearrangement of aluminosilicate nutrients around nucleation sites to result in isolated crystallites, simultaneously creating less dense areas that ultimately establish the mesopores. Step c is the point of fully transformed numerous small crystallites that are arranged into an aggregated network, the latter being arrested in its mesostructure by condensation at contact points of the particle surfaces. This aggregation creates the observed mesoporosity from interparticle voids.

Thus, under the reaction conditions employed here, highly concentrated precursor gels stimulate the formation of a large number of nucleation centers. This process is enhanced by drying the gel at an elevated temperature (60 °C), which further increases the local concentration of reactants and cationic structure-directing agents. This is in contrast to normal hydrothermal conditions where templating molecules as well as other nutrients are diluted in an additional liquid phase in the hydrogels.[52] These favorable nucleation conditions make it unnecessary to convert the precursor silica at low temperature and long reaction times, as is usually required in nanozeolite synthesis. Here, the short reaction time at high temperature transforms the abundant zeolite nuclei into fully crystalline nanosized beta crystallites without allowing for excessive growth through Ostwald ripening in the nearly dry environment. The overall fairly dense packing of the nanozeolites and the reduced water concentration as compared to normal hydrothermal synthesis are believed to control the condensation/dissolution processes critical in zeolite growth. The primary zeolite crystallites are arrested in the matrix of the dense gel, keeping each other from growing in size through close contact and finally starting to condense at the grain boundaries into self-sustaining hierarchical materials. Thus, homogeneous and stable mesopores arise from the loosely packed, very small particles after short reaction times. The zeolite nanoparticles are believed to form first at the interface between the dry gel and the steam-saturated atmosphere. In the early stages of the reaction, they can be isolated as colloidal solutions when separated from the remaining gel.

Prolonged SAC treatments induce a continuing local rearrangement assisted by partial dissolution and recrystallization events producing connected crystallite domains, easily retrievable as self-supporting grains by filtration. The mesopore size increases along with this particle growth. As a consequence, we can use an adjustment in reaction conditions to control mesopore diameter and pore volume.

Water plays a pivotal role in the crystallization mechanism, providing for a pool of concentrated nutrients affording fast nucleation, as well as for the recrystallization into ordered, more extended crystallite networks. A complete transformation of silica precursors into zeolite beta materials is thus only possible if the amount of water present in the reactor exceeds the requirements for simple saturation because water condensation in the gel is necessary. Thus, the amount of water needs to be adjusted not only for a specific temperature and reactor volume, but also for the sample loading.

In conclusion, this dense gel steam-assisted conversion results in self-assembled hierarchical zeolite beta materials that can be obtained at nearly 100% yield, and that show highly desirable properties such as very large surface areas, short diffusion distances within the primary crystallites, and large micro- and mesopore volumes of high homogeneity. Moreover, the handling of the resulting self-supported macroscopic zeolite pieces is far more convenient than that of zeolite nanoparticle suspensions. We anticipate that this efficient approach can be transferred to the synthesis of other hierarchical zeolite systems, thus providing a new generation of microporous materials with high surface areas and enhanced transport capabilities.

AUTHOR INFORMATION

Corresponding Author

bein@lmu.de; Karin.Moeller@cup.uni-muenchen.de

ACKNOWLEDGMENT

We are grateful for generous funding of this work by BASF SE, Ludwigshafen. We thank Benjamin Mandlmeier for performing

the SEM analysis and Bastian Rühle for graphical design. Helpful discussions with Matthias Thommes (Quantachrome Instruments) are highly appreciated.

REFERENCES

(1) Cejka, J., van Bekkum, H., Corma, A., Schuth, F., Eds. *Introduction to Zeolite Science and Practice*, 3rd revised ed.; Elsevier: New York, 2007; Vol. 168.
(2) Tao, Y.; Kanoh, H.; Abrams, L.; Kaneko, K. *Chem. Rev.* **2006**, *106*, 896.
(3) Meynen, V.; Cool, P.; Vansant, E. F. *Microporous Mesoporous Mater.* **2007**, *104*, 26.
(4) Perez-Ramirez, J.; Christensen, C. H.; Egeblad, K.; Christensen, C. H.; Groen, J. C. *Chem. Soc. Rev.* **2008**, *37*, 2530.
(5) Zhang, Y.; Ren, N.; Tang, Y. In *Ordered Porous Solids*; Valtchev, V., Mintova, S., Tsapatsis, M., Eds.; Elsevier: New York, 2009; Vol. 441.
(6) Egeblad, K.; Christensen, C. H.; Kustova, M.; Christensen, C. H. *Chem. Mater.* **2008**, *20*, 946.
(7) Fan, W.; Snyder, M. A.; Kumar, S.; Lee, P.-S.; Yoo, W. C.; McCormick, A. V.; Lee Penn, R.; Stein, A.; Tsapatsis, M. *Nat. Mater.* **2008**, *7*, 984.
(8) Choi, M.; Cho Hae, S.; Srivastava, R.; Venkatesan, C.; Choi, D.-H.; Ryoo, R. *Nat. Mater.* **2006**, *5*, 718.
(9) Choi, M.; Na, K.; Kim, J.; Sakamoto, Y.; Terasaki, O.; Ryoo, R. *Nature* **2009**, *461*, 246.
(10) Na, K.; Choi, M.; Park, W.; Sakamoto, Y.; Terasaki, O.; Ryoo, R. *J. Am. Chem. Soc.* **2010**, *132*, 4169.
(11) Groen, J. C.; Peffer, L. A. A.; Moulijn, J. A.; Perez-Ramirez, J. *Microporous Mesoporous Mater.* **2004**, *69*, 29.
(12) Li, X.; Prins, R.; van Bokhoven, J. A. *J. Catal.* **2009**, *262*, 257.
(13) Sommer, L.; Mores, D.; Svelle, S.; Stoecker, M.; Weckhuysen, B. M.; Olsbye, U. *Microporous Mesoporous Mater.* **2010**, *132*, 384.
(14) Holm, M. S.; Hansen, M. K.; Christensen, C. H. *Eur. J. Inorg. Chem.* **2009**, 1194.
(15) Liu, Y.; Pinnavaia, T. J. *J. Mater. Chem.* **2002**, *12*, 3179.
(16) Liu, Y.; Zhang, W.; Pinnavaia, T. J. *Angew. Chem., Int. Ed.* **2001**, *40*, 1255.
(17) Zhang, Z.; Han, Y.; Zhu, L.; Wang, R.; Yu, Y.; Qiu, S.; Zhao, D.; Xiao, F.-S. *Angew. Chem., Int. Ed.* **2001**, *40*, 1258.
(18) Shan, Z.; Zhou, W.; Jansen, J. C.; Yeh, C. Y.; Koegler, J. H.; Maschmeyer, T. *Stud. Surf. Sci. Catal.* **2002**, *141*, 635.
(19) Waller, P.; Shan, Z.; Marchese, L.; Tartaglione, G.; Zhou, W.; Jansen, J. C.; Maschmeyer, T. *Chem-Eur. J.* **2004**, *10*, 4970.
(20) Bagshaw, S. A.; Baxter, N. I.; Brew, D. R. M.; Hosie, C. F.; Yuntong, N.; Jaenicke, S.; Khuan, C. G. *J. Mater. Chem.* **2006**, *16*, 2235.
(21) Xiao, F.-S.; Wang, L.; Yin, C.; Lin, K.; Di, Y.; Li, J.; Xu, R.; Su, D. S.; Schlogl, R.; Yokoi, T.; Tatsumi, T. *Angew. Chem., Int. Ed.* **2006**, *45*, 3090.
(22) Tang, T.; Yin, C.; Wang, L.; Ji, Y.; Xiao, F.-S. *J. Catal.* **2007**, *249*, 111.
(23) Wang, L.; Zhang, Z.; Yin, C.; Shan, Z.; Xiao, F.-S. *Microporous Mesoporous Mater.* **2010**, *131*, 58.
(24) Song, J.; Ren, L.; Yin, C.; Ji, Y.; Wu, Z.; Li, J.; Xiao, F.-S. *J. Phys. Chem. C* **2008**, *112*, 8609.
(25) Zhu, H.; Liu, Z.; Kong, D.; Wang, Y.; Xie, Z. *J. Phys. Chem. C* **2008**, *112*, 17257.
(26) Valtchev, V.; Mintova, S. In *Ordered Porous Solids*; Valtchev, V., Mintova, S., Tsapatsis, M., Eds.; Elsevier: New York, 2009; Vol. 477.
(27) Tong, Y.; Zhao, T.; Li, F.; Wang, Y. *Chem. Mater.* **2006**, *18*, 4218.
(28) Lei, Q.; Zhao, T.; Li, F.; Wang, Y. F.; Hou, L. *J. Porous Mater.* **2008**, *15*, 643.
(29) Valtchev, V.; Sferdjella, S.; Kessler, H. *Stud. Surf. Sci. Catal.* **2001**, *135*, 3394.
(30) Bernasconi, S.; van Bokhoven, J. A.; Krumeich, F.; Pirngruber, G. D.; Prins, R. *Microporous Mesoporous Mater.* **2003**, *66*, 21.
(31) Perez-Ramirez, J.; Abello, S.; Bonilla, A.; Groen, J. C. *Adv. Funct. Mater.* **2009**, *19*, 164.
(32) Serrano, D. P.; Aguado, J.; Escola, J. M.; Rodriguez, J. M.; Peral, A. *Chem. Mater.* **2006**, *18*, 2462.
(33) Aguado, J.; Serrano, D. P.; Rodriguez, J. M. *Microporous Mesoporous Mater.* **2008**, *115*, 504.
(34) Na, K.; Choi, M.; Ryoo, R. *J. Mater. Chem.* **2009**, *19*, 6713.
(35) Choi, M.; Na, K.; Ryoo, R. *Chem. Commun.* **2009**, 2845.
(36) Matsukata, M.; Osaki, T.; Ogura, M.; Kikuchi, E. *Microporous Mesoporous Mater.* **2002**, *56*, 1.
(37) Rao, P. R. H. P.; Matsukata, M. *Chem. Commun.* **1996**, 1441.
(38) Rao, P. R. H. P.; Leon y Leon, C. A.; Uyama, K.; Matsukata, M. *Microporous Mesoporous Mater.* **1998**, *21*, 305.
(39) Inagaki, S.; Nakatsuyama, K.; Saka, Y.; Kikuchi, E.; Kohara, S.; Matsukata, M. *J. Phys. Chem. C* **2007**, *111*, 10285.
(40) Xu, W.; Dong, J.; Li, J.; Li, J.; Wu, F. *J. Chem. Soc., Chem. Commun.* **1990**, 755.
(41) Hari Prasad Rao, P. R.; Ueyama, K.; Matsukata, M. *Appl. Catal., A* **1998**, *166*, 97.
(42) Matsukata, M.; Ogura, M.; Osaki, T.; Raja, P.; Rao, H. P.; Nomura, M.; Kikuchi, E. *Top. Catal.* **1999**, *9*, 77.
(43) Majano, G.; Mintova, S.; Ovsitser, O.; Mihailova, B.; Bein, T. *Microporous Mesoporous Mater.* **2005**, *80*, 227.
(44) Kumar, R.; Bhaumik, A.; Ahedi, R. K.; Ganapathy, S. *Nature* **1996**, *381*, 298.
(45) Mihailova, B.; Valtchev, V.; Mintova, S.; Faust, A. C.; Petkov, N.; Bein, T. *Phys. Chem. Chem. Phys.* **2005**, *7*, 2756.
(46) Serrano, D. P.; Van Grieken, R.; Sanchez, P.; Sanz, R.; Rodriguez, L. *Microporous Mesoporous Mater.* **2001**, *46*, 35.
(47) Camblor, M. A.; Corma, A.; Valencia, S. *Microporous Mesoporous Mater.* **1998**, *25*, 59.
(48) Chen, B.; Huang, Y. *J. Phys. Chem. C* **2007**, *111*, 15236.
(49) Thommes, M. *Ser. Chem. Eng.* **2004**, *4*, 317.
(50) Ding, L.; Zheng, Y. *Microporous Mesoporous Mater.* **2007**, *103*, 94.
(51) Larsen, S. C. *J. Phys. Chem. C* **2007**, *111*, 18464.
(52) Itani, L.; Liu, Y.; Zhang, W.; Bozhilov, K. N.; Delmotte, L.; Valtchev, V. *J. Am. Chem. Soc.* **2009**, *131*, 10127.